Maximizing the resolution of a CTIS instrument

Nathan Hagen[a], Eustace L. Dereniak[a], and David T. Sass[b]

[a]Optical Sciences Center, University of Arizona, Tucson, AZ 85721
[b]U. S. Army TACOM, Warren, MI 48397

ABSTRACT

Computed Tomographic Imaging Spectrometry (CTIS) is a technique which has been around for over a decade, providing snapshot measurements of datacubes as large as (x,y,λ) = (100,100,300). We discuss the difficulties with maximizing the resolution of a CTIS instrument and some new grating design ideas for realizing performance improvements.

Keywords: spectrometry, imaging spectrometry, CTIS, computed tomography

1. COMPUTED TOMOGRAPHY IMAGING SPECTROMETRY (CTIS)

The data acquired by an imaging spectrometer is represented as a three-dimensional volume, the *datacube*. Conventional imaging spectrometers are inherently sensitive to a one-, two-, or three-dimensional subset of the datacube, and must scan out the remaining dimensions in order to obtain a complete data set. For example, a camera with a narrow-band filter could be used to obtain a single horizontal slice through the hypercube. In this slice x and y vary while λ is fixed at the wavelength passed by the filter. The entire three dimensions could be swept out by swapping in filters with different transmission wavelengths in tandem with an analyzer and a rotating retarder. Similar examples can be made for other systems, such as slit spectrometers and whisk broom scanners (see Fig. 1).

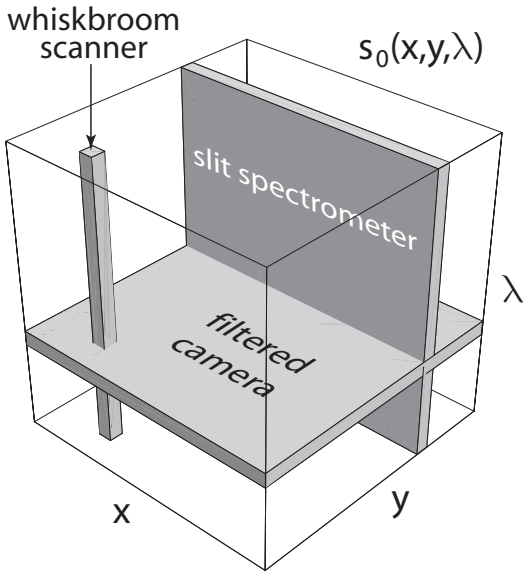

Figure 1. The lower-dimensional volumes which various spectrometer types are capable of imaging without scanning.

The CTIS design (shown in Fig. 2 below) involves imaging through a 2D transmission grating (Fig. 3), with the result that the imaged scene is dispersed into a rectangular array of prismatic images (Fig. 4).[1,2] By placing a field stop at a conjugate plane to the FPA, we can limit the spatial extent of the scene imaged, allowing the prismatic images to be spatially separated. The disperser is a kinoform — a surface relief grating — fabricated from PMMA (plastic), where each individual cell of the grating is designed to produce the desired dispersion pattern for the spectral range of the instrument. Then the designed cell pattern is then replicated over the clear aperture to produce the final grating design.[3,4]

For an example calculation of CTIS system parameters, we can use the visible-spectrum CTIS which we have constructed, which uses a 2048×2048 pixel B/W CCD camera, and the grating has been designed to produce a 5×5 CTIS diffraction pattern. The undiffracted (zero-order) image in the center of the focal plane array (FPA) provides a measure of the spatial resolution of the datacube, which in this case has dimensions of 75×75 pixels. The best spectral sampling of the object is provided by the outermost diffraction orders, where the spectral projections are the most spread out. Here, the outer diffraction orders in the prototype system are smeared (spatially and spectrally multiplexed) across a range of 470 pixels in both the horizontal and the

Further author information: E-mail: nhagen@optics.arizona.edu

Imaging Spectrometry XI, edited by Sylvia S. Shen, Paul E. Lewis,
Proc. of SPIE Vol. 6302, 63020L, (2006) · 0277-786X/06/$15 · doi: 10.1117/12.680750

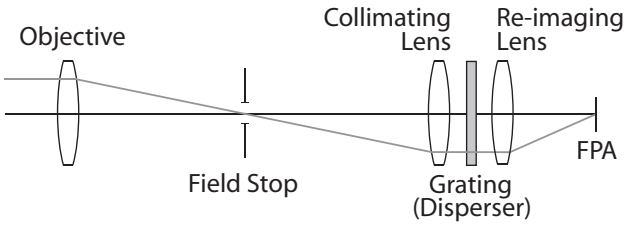

Figure 2. The CTIS optical layout.

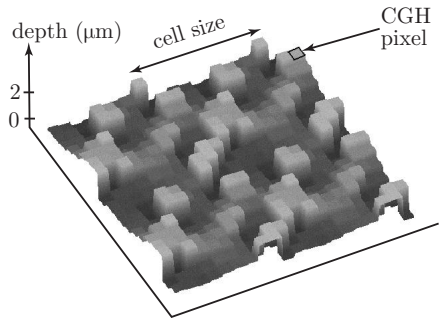

Figure 3. The surface relief pattern of the 2D grating ("disperser"). Shown here is a section of the grating (2 cells × 2 cells), where each cell comprises 10×10 "phasels".

vertical directions (Fig. 4). Removing the spatial component (75 pixels), gives the spectral dispersion alone, 395 pixels. Since the sampling of the data occurs along the diagonal of the FPA, the number of pixels involved, and thus the sampling rate, is increased by a factor of $\sqrt{2}$, so that we can approximate the ideal spectral sampling achievable by this setup as $395 \times \sqrt{2} \approx 560$ spectral bands in the visible region, giving a spectral sampling rate of $\sim$0.6 nm/pixel.

In practice, however, the *achievable* spectral resolution is strongly dependent on the SNR of the image and on the amount of spatial-spectral multiplexing present in the image (*i.e.* point sources have minimal multiplexing, and thus are much easier to reconstruct accurately). The noise dependence is most apparent in the fact that with each subsequent iteration of a reconstruction algorithm, the noise is slightly amplified, so that the SNR of the reconstructed datacube trades off with resolution enhancement.

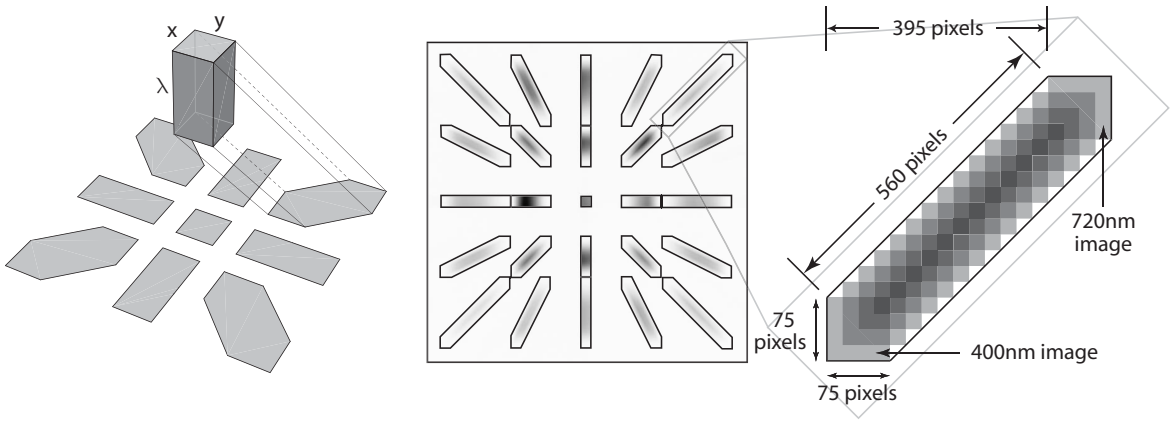

Figure 4. A typical image from a CTIS FPA, with outlines of each diffracted order superimposed, shown with the computed-tomographic model (at left) of projections of the datacube onto the FPA. The blowup of the corner diffracted order (at right) gives a figurative illustration of the spatial and spectral multiplexing.

To develop a method for reconstructing the dispersed prismatic images into a single datacube, we can start with the linear imaging equation[5]

$$\mathbf{g} = \mathbf{H} \quad \mathbf{f}(x, y, \lambda)$$

image (output) — system operator — object (input)

If we lexicographically order the pixel information of our detected image into a long 1D vector (indexed by m) and do the same for each voxel in the datacube (indexed by n), then each element H_{mn} of the system matrix

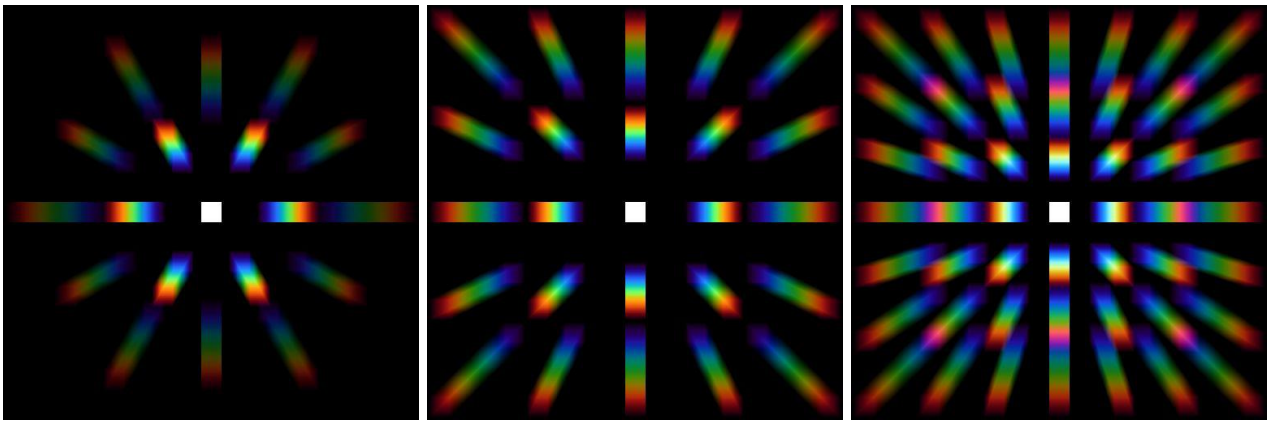

(a) 3Cos Design (b) 5×5 design (c) 7×7 design

Figure 5. Past CTIS grating designs, showing the pattern at the focal plane for an object with a uniform datacube.

maps the sensitivity of each voxel in the datacube to each pixel in the image. The full system matrix $\mathbf{H}$ can then be calibrated using a series of detected images $\mathbf{g}$ of a quasi-monochromatic point-source f_n (*i.e.* a small-diameter optical fiber placed directly into the field stop and illuminated by a monochromator). Performing this step at each wavelength band and each spatial position fills in the matrix elements of $\mathbf{H}$. The reconstruction process used to estimate the object $\mathbf{f}$ from a measured image $\mathbf{g}$ requires some kind of inversion of the system matrix. Past work in our group has concentrated on two iterative reconstruction algorithms, based on the Expectation Maximization (EM) method or the Multiplicative Algebraic Reconstruction Technique (MART):[6]

$$\textbf{EM}: \boxed{\hat{f}_n^{(k+1)} = \frac{\hat{f}_n^{(k)}}{\sum_m H_{mn}} \sum_{m=1}^{M} H_{nm}^{\mathsf{T}} \frac{g_m}{\left(\mathbf{H}\hat{\mathbf{f}}^{(k)}\right)_m}} \qquad \textbf{MART}: \boxed{\hat{f}_n^{(k+1)} = \hat{f}_n^{(k)} \frac{\left(\mathbf{H}^{\mathsf{T}}\mathbf{g}\right)_n}{\left(\mathbf{H}^{\mathsf{T}}\mathbf{H}\hat{\mathbf{f}}^{(k)}\right)_n}}$$

where $\hat{f}$ indicates an *estimate* of the object's datacube.

2. ALTERNATIVE CTIS DESIGNS: CLUES FROM THE FOURIER SLICE THEOREM

The snapshot CTIS technique allows the tradeoff of spatial for spectral information of the object. In order to improve on CTIS disperser designs, we would like to know how far we can push this tradeoff and what the design constraints are. The original CTIS disperser design used a set of three crossed cosine gratings.[?] Two difficulties with this design were that its was very sensitive to errors in the relative angular orientation of the three gratings, and that the zero-order dominated the image, limiting the ability to capture good SNR data (see Fig. 5*a* below). Later disperser designs used techniques from computer-generated holography to produce a kinoform disperser with a 5×5 rectangular pattern which better matched the rectangular format of the detector array (Fig. 5*b*). Additionally, the kinoform design provided additional design flexibility such that the outer diffraction orders could be enhanced by greater diffraction efficiency, while the efficiency of the inner orders (and zero order) could be suppressed. This allowed for CTIS images with a much more uniform light distribution and better SNR.

From the analogy of the CTIS measurement technique to that of computed tomography (measuring a 3D object, the datacube, from its 2D projections) as implied by Fig. 4, we can make use of an important mathematical theorem from the computed tomography literature: the Fourier Slice Theorem. This theorem states that the Fourier Transform of a single projection (a 2D object) is equivalent to the Fourier Transform of the original object (in 3D) evaluated along a plane which passes through the origin.[5] Thus, each footprint for a given CTIS design corresponds to sampling the Fourier cube (the Fourier Transform of the object's datacube) along a single plane. The effect of having many different projections is to sample along a number of planes tilted at different angles, but all of which pass through the origin in Fourier space. Thus, using a continuous model to approximate

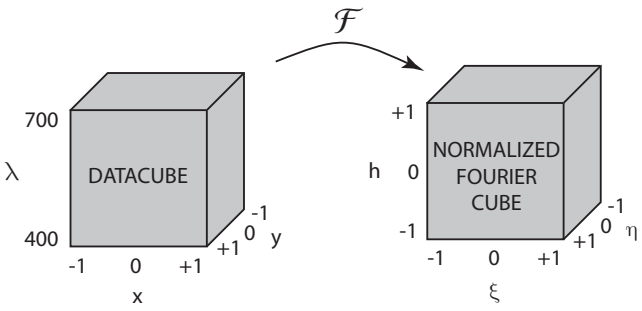

Figure 6. The nomenclature used for the axes in forward and reciprocal space. The h-axis is normalized such that if there are twice as many wavelength bands in the datacube as there are pixels in the spatial dimensions of the cube, then the h-axis will have a frequency range of -2 to $+2$.

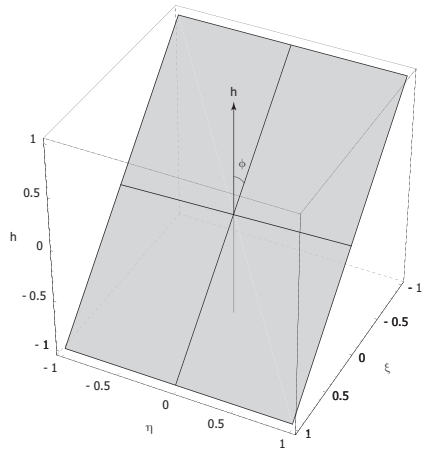

Figure 7. A plane in normalized Fourier space (h is the Fourier variable corresponding to the λ dimension of the datacube).

the behavior of a discrete measurement system, for each CTIS design we can construct a diagram showing all of the planes in Fourier space which are sampled by the instrument. The basic idea is illustrated in Figs 6 & 7.

The evolution of CTIS disperser designs has largely consisted of a steady increase in the number of diffraction orders. The original CTIS design, employing three crossed cosine gratings ("3Cos"), used multiples of $+1$ and -1 diffraction orders. The next CTIS design (the "5×5") used a kinoform to generate a diffraction pattern using the $+2, +1, 0, -1$ and -2 orders in the vertical and horizontal directions. A later design (the "7×7") took a step further and superimposed a total of 49 spectral footprints onto the focal plane array, generated by taking the $+3$ through -3 diffraction orders for both vertical and horizontal directions. Making use of the Fourier Slice Theorem, we can construct Fourier slice diagrams for each design and examine the sampling in the Fourier domain. These diagrams are shown in Fig. 8.

Once we note that most of the Fourier cube frequencies which are sampled by the inner diffraction orders are *also* sampled by the higher diffraction orders (since the planes are heavily overlapping), it becomes apparent that we can equivalently sample the Fourier cube by making use of only outer diffraction orders, but increasing the number of projection angles. This is the idea underlying the radial design shown in Fig. 8*d*,*h*–*j*. This design uses only the $+1$ and -1 diffraction orders, but provides for 31 projections.

A distinguishing feature to every CTIS design is the cone-shaped region, centered on the reciprocal-wavelength axis h, where none of the frequencies of the Fourier cube are sampled. This is a well-known problem for limited-angle tomography, and one which can cause considerably difficulty for accurate reconstruction. This provides an important characterization of the various CTIS designs: the size of the missing cone. In each of the Fourier representations, the geometry of the sampling planes allows us to obtain the missing cone angle, represented by ϕ. (Note that this angle appears exaggerated due to the compressed vertical axis in the figures.)

In order to design a disperser for this new radial design pattern, the design method for the disperser needs modification. Past "rectangular" CTIS designs (such as the 5×5 and 7×7 designs) used a small unit cell, usually of 8×8 phasels. Using a variant of the well-known Gerchberg-Saxton approach (also known as phase retrieval), the desired dispersion pattern can be used to estimate the phases in the unit cell, assuming a planewave incident on the disperser. Once the unit cell design is complete, the cell phases are translated into physical etch depths into the surface relief of the grating material, and the pattern is replicated across the clear aperture of the beam.[6] Since the "radial" design no longer has a direct correspondence between elements of a unit cell and elements of the dispersion pattern, the unit cell approach is no longer possible. However, the phase retrieval method is still valid, but must instead be performed over the entire disperser rather than a single unit cell. The desired dispersion pattern is set to be a series of narrow Gaussian spots, at diffraction angles appropriate for the optical system design (Fig. 9). Example greyscale maps of the 5×5 and Radial CTIS designs are shown in Figs 10 & 11.

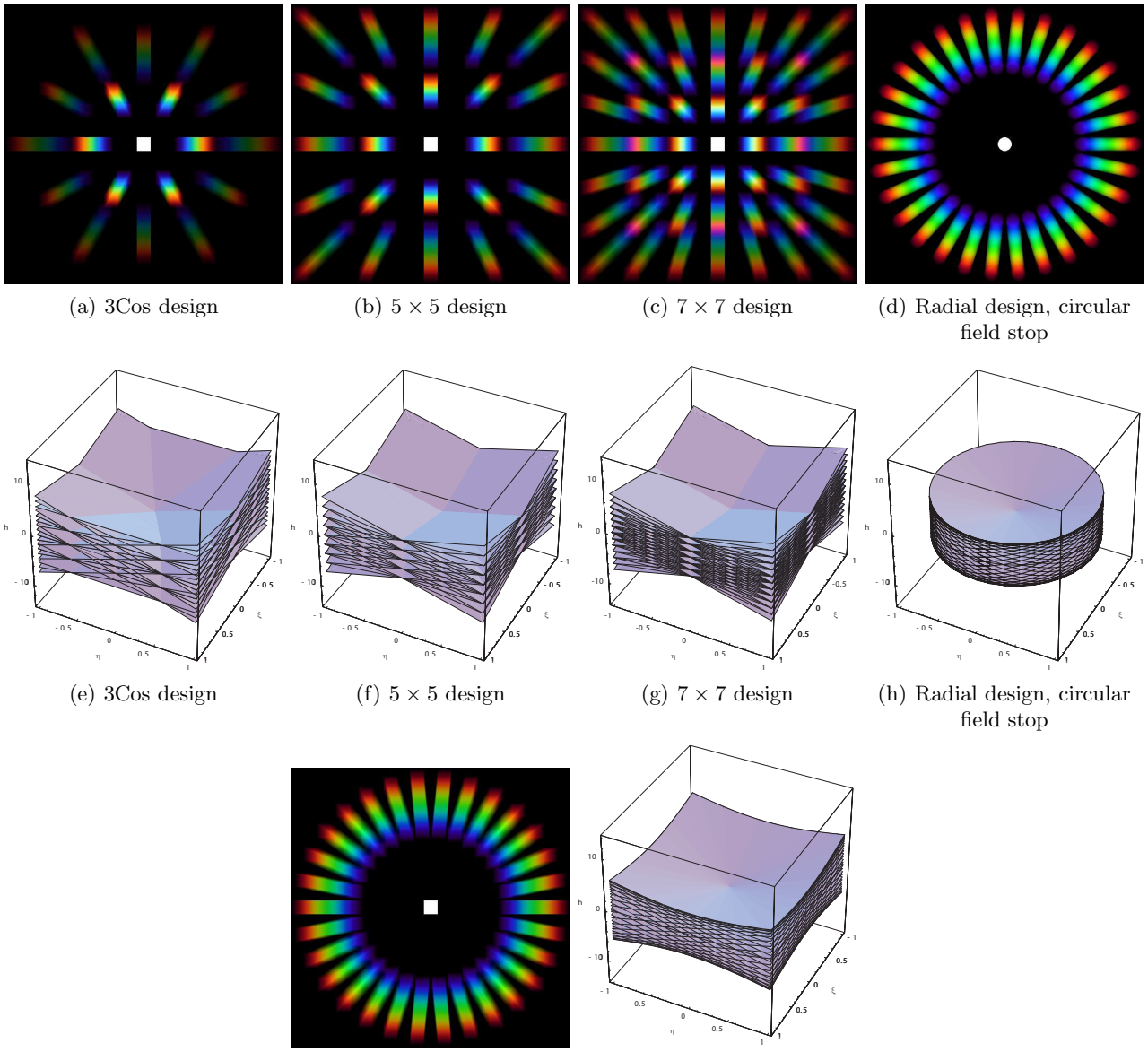

(a) 3Cos design (b) 5×5 design (c) 7×7 design (d) Radial design, circular field stop

(e) 3Cos design (f) 5×5 design (g) 7×7 design (h) Radial design, circular field stop

(i) Radial design, square field stop (j) Radial design, square field stop

Figure 8. CTIS menagerie: the linear designs and Fourier slice diagrams. Note that the central cone angle looks exaggerated because the vertical axis of the Fourier slice diagrams has been greatly compressed.

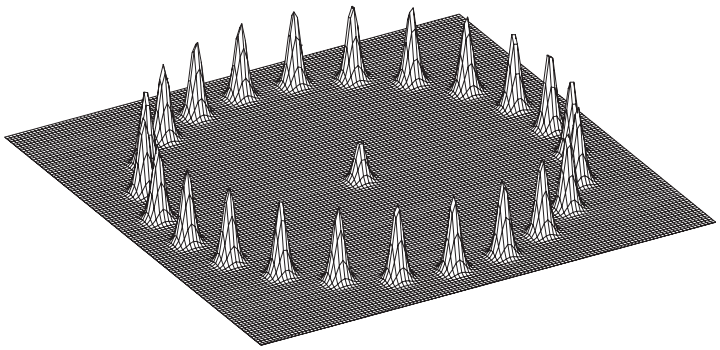

Figure 9. The desired diffraction pattern at the focal plane for a radial CTIS design. The Gaussian profile widths have been exaggerated in order to make them more visible.

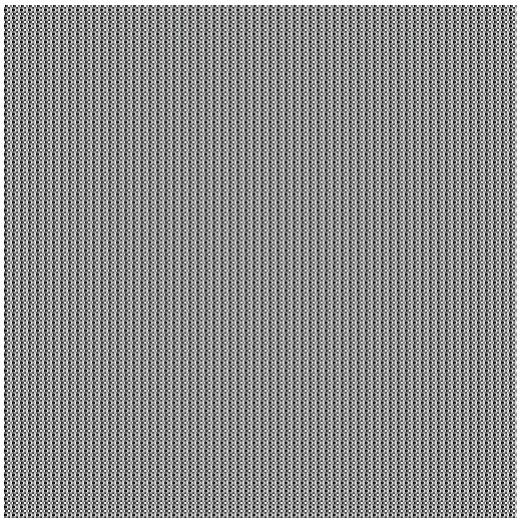

Figure 10. Greyscale map of the CGH pixel phases for the 5×5 CTIS design (white = 2π, black = 0).

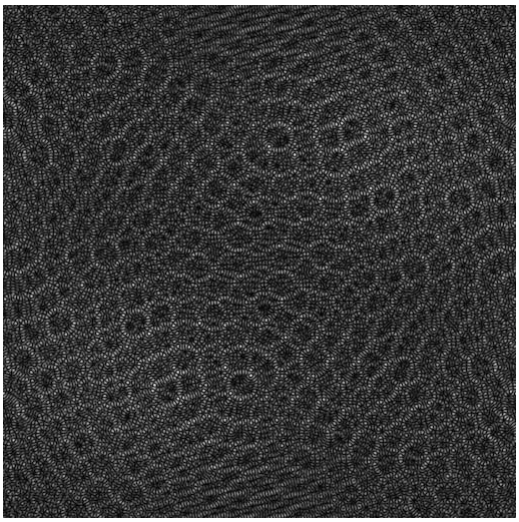

Figure 11. Greyscale map of the CGH pixel phases for the Linear radial CTIS design (white = 2π, black = 0).

3. IMPROVING CTIS DESIGN: NONLINEAR DIFFRACTION

An important constraint limiting CTIS disperser designs is that the dispersion angle is (approximately) linear with wavelength. That is, if we wish to maximize the spectral resolution of a CTIS instrument, we can push the red end of the spectrum all the way out to the edge of the focal plane, but the blue end of the spectrum cannot be pulled all the way in towards the center of the diffraction pattern. If we are using the visible wavelength spectrum (400 nm–700 nm) then the blue end of the spectrum is diffracted a distance which is 4/7ths that of the red light, with the intervening distance empty (Fig. 12). If the limitations of physics can be placed aside for a moment, we can consider the potential advantages to CTIS spectral resolution for grating designs which achieve *nonlinear* dispersion angle with wavelength.

If we allow a given CTIS design to map diffraction angles nonlinearly with wavelength, then we can, for example, take a simple 3×3 CTIS design and almost double the spectral resolution by bringing the short-wavelength end of the spectrum close to the center of the diffraction pattern. Or, we can do the same thing with the radial design, with some tradeoff between the number and length of the projections (Fig. 14*b*–*c*,*f*–*g*). Taking a step further, if the diffraction angle as a function of wavelength can be varied in 3D, and yet maintain itself as a continuous function, then we can wrap the radial design into a spiral (Fig. 14*d*,*h*), allowing for further increases in spectral sampling.

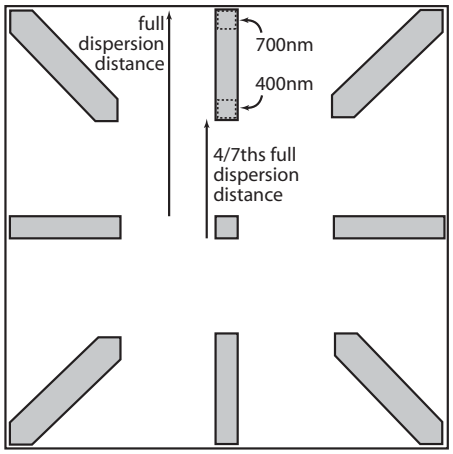

Figure 12. The maximum achievable dispersion of a grating designed for linear dispersion in the visible spectrum range, 400 nm–700 nm.

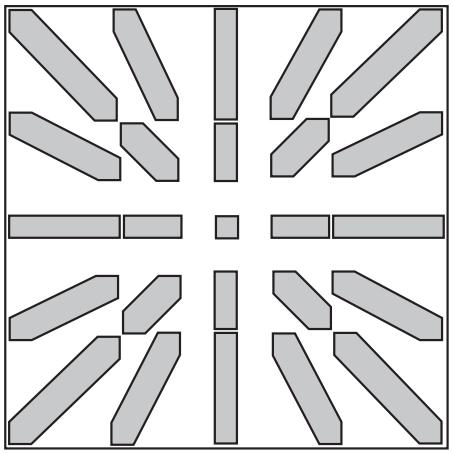

Figure 13. The current 5×5 dispersion CTIS design configuration, optimized for maximum spectral dispersion. The inner diffraction orders fit entirely inside the set of outer orders.

Returning to the limitations that physics places on disperser design, how can the improved performance of the nonlinear designs possibly be realized? For the case of a 1D disperser (such as in a typical prism spectrometer), nonlinearity of the dispersion angle can be controlled by modifying the prism glass material and by converting it into a grism. Unfortunately, this process does not transfer to 2D dispersers. However, we can take note of the methods used in holographic storage, where various wavelengths and incidence angles can be encoded simultaneously into a holographic medium. In the same way, a volume holographic grating can be designed which encodes a fringe field that simultaneously constrains the transmitted wavelength and its angle of diffraction. If many of these fringe fields can be simultaneously written into the medium while maintaining little crosstalk, then simple nonlinear designs (with limited numbers of angles and wavelengths) should be achievable. The complexity of such a volume hologram for a full CTIS design, however, appears to be infeasible with current technology.

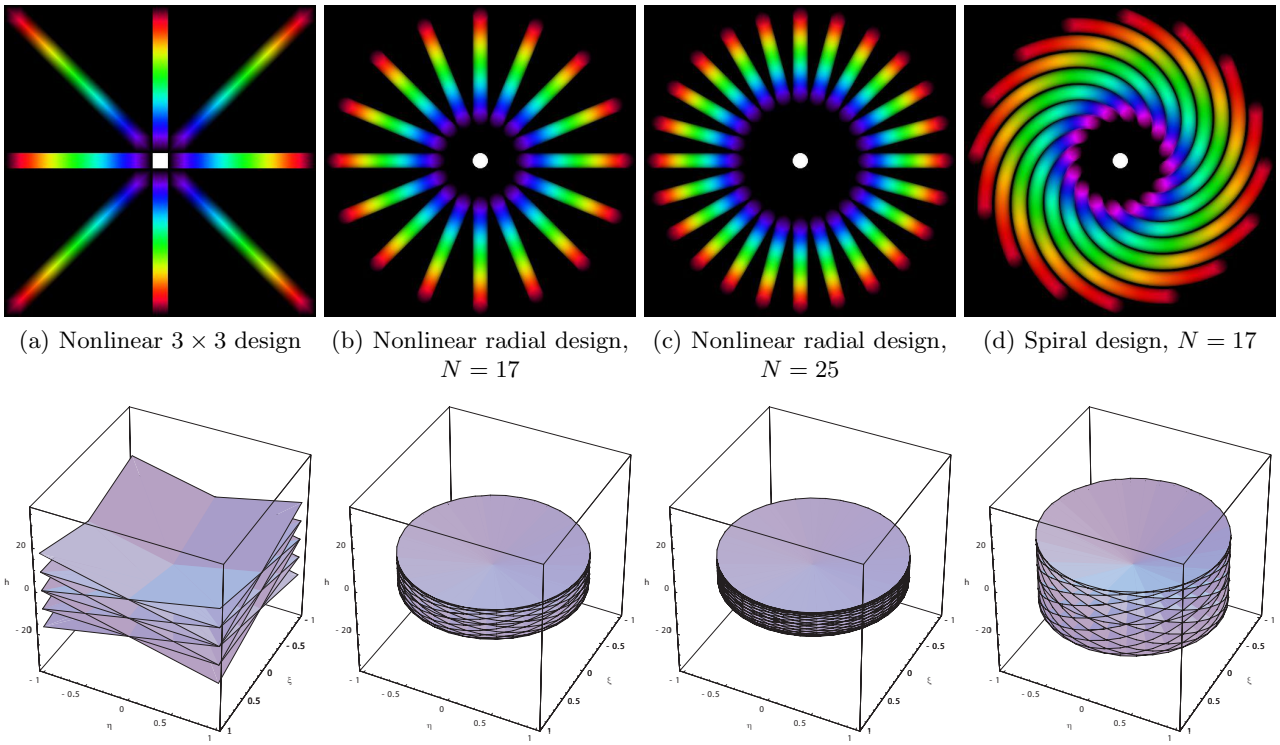

(a) Nonlinear 3×3 design (b) Nonlinear radial design, $N = 17$ (c) Nonlinear radial design, $N = 25$ (d) Spiral design, $N = 17$

(e) Nonlinear 3×3 design (f) Nonlinear radial design, $N = 17$ (g) Nonlinear radial design, $N = 25$ (h) Spiral design, $N = 17$

Figure 14. CTIS menagerie: the nonlinear designs and corresponding Fourier slice diagrams. Note that the vertical axes in the slice diagrams differ from those of Fig. 8. And here, too, the central cone angles appear exaggerated because the vertical axes of the Fourier slice diagrams have been greatly compressed.

4. IMPROVING CTIS DESIGN: METRICS FOR DISPERSER DESIGNS

Having a set of various CTIS designs, we need to know the performance differences between these designs. In order to compare them, we can first construct a set of metrics based on desirable characteristics. There are six important metrics for characterizing the various CTIS designs:

1. *Spatial Dimension, D*: D describes the number of pixels in x and in y, if we assume that the datacube is square, for sampling the spatial distribution in the object.

2. *Number of Projections, P*: although P is often a parameter which is *chosen* for a given design, increasing the number of projections improves reconstruction quality. (Medical imaging systems typically use hundreds of projection angles for performing reconstructions.)

3. *Spectral Sampling Number, L*: if spectral resolution is particularly important for a given CTIS system, then the number of spectral samples is an important metric closely related to the realizable spectral resolution of the system.

4. *Fill Factor*: in order to maximize its ability to measure the object datacube, a good CTIS design will maximize the use of space on the focal plane array (and minimize the number of unused pixels).

5. *Blur Factor*: with an increase in the blurring and mixing of spatial and spectral components of the datacube onto the pixels of the FPA, the theoretically achievable spatial and spectral resolution decreases. Thus, a measure of this blurring/mixing provides a metric for the distance between what an actual design can achieve and what its ideal performance is. A rough way to estimate the blurring which occurs in a given

Table 1. *Comparison of the CTIS designs.* $\boldsymbol{D}$ = dimension of the zero order, $\boldsymbol{P}$ = number of projections, $\boldsymbol{L}$ = pixels of spectral dispersion, $\boldsymbol{\phi}$ = missing cone angle (in degrees). Each of the designs tabulated here assume the use of a 2048 × 2048 pixel FPA, measuring data in the visible spectrum (400 nm–700 nm).

Design Parameters			Design Metrics				
Design Type	$\boldsymbol{D}$	$\boldsymbol{P}$	$\boldsymbol{L}$	**Fill**	**Blur**	$\boldsymbol{\phi}$	**Notes**
Linear Designs							
3Cos	100	19	551	0.22	163	10.30	
5×5	100	25	526	0.35	99	9.73	(430nm – 700nm)
Radial Linear	100	32	416	0.48	68	13.55	
7×7	100	49	526	0.59	97	9.73	(430nm – 700nm)
Nonlinear Designs							
3×3 Nonlinear	100	9	1208	0.27	97	4.73	
Spiral	100	13	2268	0.60	79	3.87	
Radial Nonlinear	100	13	758	0.30	78	7.53	
Spiral	100	25	1050	0.64	97	5.45	
Radial Nonlinear	100	25	548	0.46	72	10.36	

CTIS system is to determine the mean number of voxels which a given pixel on the FPA is sensitive to. (This is equivalent to estimating the width of the PSF for a given pixel via the backprojection, $\mathbf{H}^{\mathsf{T}}$).

6. *Missing cone angle*, $\boldsymbol{\phi}$: while this metric is dependent on the spectral sampling rate L, and on the spatial sampling rate D, the missing cone angle provides another convenient way of comparing CTIS designs.

A set of CTIS designs is shown in Table 4, together with the design parameters relevant to each. In the tabulated data, it should be mentioned that since the spiral designs cannot be represented by a linear projection, the spatial-spectral footprints on the array cannot be represented as sampling a planar region in Fourier space (*i.e.* the Fourier Slice Theorem is no longer valid). However, in order to make some kind of comparison with the other designs here, a spiral pattern is assumed to be represented by an equivalent radial design pattern — a nonlinear radial pattern with the same number of projections and the same spectral resolution as that possessed by the spiral design.

While the six merit functions (D, P, L, $fill$, $blur$, and ϕ) are all useful for characterizing the different possible disperser designs, they compete against each other and thus cannot provide an objective measure to determine which design provides the best performance. To provide such a measure, we have constructed a detailed simulation of a CTIS system, comprising ideal (aberration-free) optics, an ideal disperser, and a noiseless detector array. "Measuring" a series of object datacubes with this system, and then performing a reconstruction, we can obtain an rms measure of error for each given disperser design. Specifically, the metric we use is an "error fraction" ϵ_{f}, defined as

$$\epsilon_{\mathrm{f}} = \left[\frac{1}{N} \sum_{n} \left(\frac{f_n - \hat{f}_n}{f_n} \right)^2 \right]^{1/2} , \tag{1}$$

where $\mathbf{f}$ is the input datacube, $\hat{\mathbf{f}}$ is the reconstructed datacube estimate, and N is the number of voxels in each. (Those terms in the sum where $f_n = 0$ are set to zero). Thus, if $\hat{f}_n$ consistently under- or over-estimates f_n by 10% then the resulting error fraction will be 0.10. Since the types of objects used in the calculations here differ from each other greatly, this metric provides a number which is much easier to compare across the various designs.

Five different objects, in order of difficulty for CTIS, were used in the following simulation:

1. *Narrowband pointsource*: the easiest of objects for CTIS to reconstruct, this datacube represents an object which has a Gaussian spectral profile (FWHM = 20 nm) and a 2D Gaussian spatial profile (FWHM = 4 pixels).

2. *Uniform*: another easy, but this time somewhat unrealistic, object for CTIS to measure is one which is spatially uniform as well as spectrally uniform (artificial white).

3. *Whitelight pointsource*: a more realistic object, somewhat simplified here, is that of a whitelight (*i.e.* spectrally uniform) pointsource.

4. *Channeled spectrum uniform*: some CTIS systems integrate their measurements with channeled spectropolarimetry in order to obtain polarimetric information.[7] This object is a simple example of the type of object that may be seen in such a system when performing photoelasticity or retardance measurements on a transparent sample. The object is spatially uniform but modulated at a constant frequency along the wavelength dimension. (Note that this places the object entirely within the CTIS missing cone.)

5. *UA logo*: in order to generate a datacube which is at the same time noise free and yet possesses a complex spatial and spectral structure, we used the Univ. of Arizona color logo, taking the sRGB standard to estimate the spectral shape of each pixel in the image generated by a CRT display (thus generating a full datacube from an RGB image). While the spectra thus generated are relatively smooth, the spatial profile exhibits sharp changes.

The results of passing these example datacubes through the various CTIS designs (each with one of the disperser designs of Table 4, excepting the last two) are shown in Fig. 15. For the easier datacube examples, each of the disperser designs gives equivalent accuracy in the reconstruction. For the more difficult datacubes, the result at first appear more ambiguous. What we see is that for the channeled spectrum datacube, those disperser designs which have the best spectral sampling (averaged across all the P projections) produce the best results, and thus the 3Cos and linear radial designs — having the worst and 2$^{\text{nd}}$ worst spectral sampling rates — have the worst performance, while the 3×3 NL and the Spiral designs have the best performance. For the "UA logo" datacube, however, the nonlinear designs perform badly, a result of the fact that for this datacube it is the spatial information which is difficult to reconstruct, so that the number of projections P becomes more important than the spectral sampling L. Thus, for the "UA logo" cube, the radial and 7×7 designs do very well, whereas the nonlinear designs do poorly because of their limited number of projections.

The large value of the error fraction for the more difficult designs is partly an artifact of the choice of merit function. For the most part, even when the error fraction is 50%, the proper form of the datacube is retained, though the features are generally smoothed out, as if passed through a low-pass filter. The error metric ϵ_{f}, while a good starting point, is not the most accurate method for assessing the performance of the instrument. A better approach would be to select a task for the system, such as detecting the presence or absence of an object in a noisy background, or estimating the retardation present in a transparent sample. This extension is the subject of ongoing research.

5. CONCLUSIONS

The "radial" CTIS disperser pattern is a new design that provides different capabilities for CTIS systems, which may prove useful for systems where spatial resolution in the reconstructed datacubes is more important than the spectral resolution. While the nonlinear designs presented here show huge promise in their spectral resolution, this advantage decreases rapidly as the number of projections is increased, so that for good spatial resolution (relative to, say, the 5×5 disperser pattern design), the spectral resolution advantage becomes small. While this tradeoff may be useful for CTIS systems incorporating channeled spectropolarimetry (which have strict spectral resolution requirements), it is unlikely to be useful for other CTIS instruments.

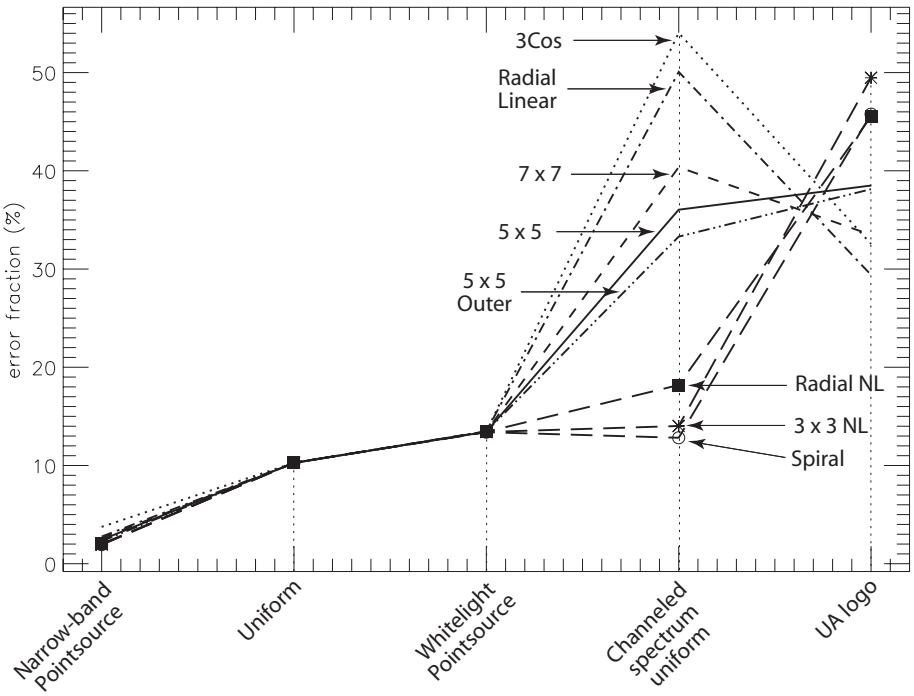

Figure 15. The error fraction due to reconstruction of the five example datacubes for each of 7 different CTIS disperser designs.

REFERENCES

1. T. Okamoto and I. Yamaguchi, "Simultaneous acquisition of spectral image information," *Opt. Lett.* **16**(16), pp. 1277–1279, 1991.
2. M. R. Descour, C. E. Volin, E. L. Dereniak, K. J. Thome, A. B. Schumacher, D. W. Wilson, and P. D. Maker, "Demonstration of a high-speed nonscanning imaging spectrometer," *Opt. Lett.* **22**(16), pp. 1271–1273, 1997.
3. M. R. Descour, C. E. Volin, E. L. Dereniak, T. M. Gleeson, M. F. Hopkins, D. W. Wilson, and P. D. Maker, "Demonstration of a computed-tomography imaging spectrometer using a computer-generated hologram disperser," *Applied Optics* **36**(16), pp. 3694–98, 1997.
4. C. E. Volin, M. R. Descour, and E. L. Dereniak, "Design of broadband-optimized computer-generated hologram dispersers for the computed-tomography imaging spectrometer," in *Imaging Spectrometry VII*, D. H. Goldstein, D. B. Chenault, W. G. Egan, and M. J. Duggin, eds., *Proc. SPIE* **4481**, pp. 377–387, 2002.
5. H. H. Barrett and K. Meyers, *Foundations of Image Science*, Wiley, New York, 2003.
6. C. E. Volin, *Portable snapshot infrared imaging spectrometer*. PhD thesis, University of Arizona, Tucson, Arizona, 2000.
7. N. Hagen, E. L. Dereniak, and D. T. Sass, "Visible snapshot imaging spectro-polarimeter," in *Polarization Science and Remote Sensing II*, J. A. Shaw and J. S. Tyo, eds., *Proc. SPIE* **5888**(10), 2005.